Infuence of correlation effects on the of magneto-optical properties of half-metallic ferromagnet NiMnSb

S. Chadov, J. Minár, and H. Ebert

Dept. Chemie und Biochemie, Physikalische Chemie,

Universität München, Butenandtstr. 5-13, D-81377 München, Germany

A. Perlov

Accelrys, 334 Cambridge Science Park, CB4 0WN Cambridge, England

L. Chioncel †

Institute of Theoretical Physics, Technical University of Graz, A-8010 Graz, Austria

M.I. Katsnelson

University of Nijmegen, NL-6525 ED Nijmegen, The Netherlands

A.I. Lichtenstein

Institute of Theoretical Physics, University of Hamburg, Germany

Abstract

The magneto-optical spectra of NiMnSb were calculated in the framework of the Local Spin Density Approximation (LSDA) combined with Dynamical Mean-Field Theory (DMFT). Comparing with results based on plain LSDA, an additional account of many-body correlations via DMFT results in a noticably improved agreement of the theoretical Kerr-rotation and ellipticity spectra with corresponding experimental data.

PACS numbers: 78.20.Ls, 71.20.Be, 71.15.Rf

Since the discovery of the giant magneto-optical Kerr effect (MOKE) in PtMnSb [1] magneto-optical properties became an important issue for the Mn-based family of Heusler alloys [2, 3, 4, 5, 6, 7, 8, 9, 10]. However, despite of the similar structure, the group of isoelectronic alloys PtMnSb, NiMnSb and PdMnSb show quite different maximum amplitudes in their MOKE spectra [1, 2]. A theoretical description of the observed difference of the MOKE spectra became possible within *ab-initio* band-structure calculations [8, 10, 11, 12]. However, although the various calculated MOKE spectra give reasonable qualitative agreement with experiment, one can notice that there exist several systematic discrepancies generally ascribed to the use of local spin density approximation (LSDA). In particular, for NiMnSb, one can see that the low-energy peak of the Kerr rotation spectra at 1.4 eV is shifted to a regime of 1.6-2 eV. Also there is a noticable deviation of the amplitude for the peak at 4 eV as well as in the intermediate energy regime. Among other reasons, the discrepancies encountered in LSDA-based results could appear due to an insufficient treatment of electronic correlations. For example, as it was shown for bcc Ni [13, 14], the account of local dynamical correlations is essentially important for a proper description of its MOKE spectra. In the case of NiMnSb the main contribution to the optical transitions comes from the d-shell of Mn which supplies the unoccupied part of the density of states (DOS). At the same time d-electrons of Mn should be treated as locally-correlated [15]. Based on this supposition one can expect an improvement of MO spectra in NiMnSb by an appropriate account of local correlation effects for the Mn d-shell in band-structure calculations. In the present work the latter is implemented within the so-called Dynamical Mean Field Theory approach (DMFT) [16].

In our calculations the central quantity is the optical conductivity tensor $\sigma_{\lambda\lambda'}$, as all optical and magneto-optical properties, can be expressed through its cartesian components ($\lambda = \{\mathrm{x}, \mathrm{y}, \mathrm{z}\}$). In particular for the complex Kerr angle, that combines Kerr rotation θ_{K} and ellipticity ε_{K}, the following expression can be used [17]:

$$\theta_{\mathrm{K}}(\omega) + \mathrm{i}\,\varepsilon_{\mathrm{K}}(\omega) \approx \frac{-\sigma_{\mathrm{xy}}(\omega)}{\sigma_{\mathrm{xx}}(\omega)\sqrt{1 + \dfrac{4\pi\mathrm{i}}{\omega}\,\sigma_{\mathrm{xx}}(\omega)}}\,. \tag{1}$$

In order to calculate the optical conductivity we use the expression for the hermitian component derived for the zero-temperature case [18] by implementing the Green's function

formalism in Kubo's linear response theory [19]:

$$\sigma^{(1)}_{\lambda\lambda'}(\omega) = -\frac{1}{\pi V}\int\limits_{\epsilon_{\rm F}-\hbar\omega}^{\epsilon_{\rm F}} {\rm d}\epsilon \ {\rm Tr}\left\{\hat{J}^{\lambda}\,\Im G(\epsilon+\hbar\omega)\,\hat{J}^{\lambda'}\,\Im G(\epsilon)\right\}, \tag{2}$$

where V is the volume of the spatial averaging, $\hat{J}^{\lambda}$ is the current-density operator. $\Im G(\epsilon)$ stands for the antihermitian part of the retarded one-electron Green's function. The hermitian part of the conductivity tensor $\sigma^{(2)}_{\lambda\lambda'}(\omega)$ can be obtained via the Kramers-Kronig relations.

Formulation (2) is used because it allows to include straightforwardly all correlations in the one-particle Green's function via the Dyson equation:

$$\left[\epsilon - \hat{H}_0 - \hat{\Sigma}(\epsilon)\right]\hat{G}(\epsilon) = \hat{I}\,, \tag{3}$$

where $\hat{H}_0$ is LSDA-based one-particle Hamiltonian including the kinetic energy, electron-ion interaction and the Hartree potential, while the self-energy operator $\hat{\Sigma}$ describes all static and dynamic effects of electron-electron exchange and correlations. The most popular approximation nowadays for the self-energy is DMFT which introduces it as a local, energy-independent exchange-correlation potential $V_{\rm xc}(r)$. As the introduction of such an additional potential does not change the properties of H_0 we will incorporate this potential to $H_{\rm LSDA}$ and subtract this term from the self-energy operator. This means that the self-energy Σ describes exchange and correlation effects not accounted for within LSDA.

The most straightforward and accurate way to solve Eq. (3) is to use the Korringa-Kohn-Rostoker Green's function method (KKR-GF) [20]. However subsequent calculations of optical properties within the KKR-GF method become very time-consuming due to the energy-dependent matrix elements of the current-density operator. A possibile alternative is to use the so-called variational, or fixed basis-set methods. Within such an approach the Green's function is represented as a sum over energy independent basis functions $|i\rangle$:

$$\begin{aligned} G(\epsilon) &= \sum_{ij} |i\rangle\langle i| \frac{1}{\epsilon - H_{\rm LSDA} - \Sigma(\epsilon)} |j\rangle\langle j| \\ &= \sum_{ij} |i\rangle G_{ij}(\epsilon)\langle j|\,, \end{aligned} \tag{4}$$

with the Green's function matrix defined as

$$G_{ij}(\epsilon) = \left[\langle i|j\rangle\epsilon - \langle i|\hat{H}_{\rm LSDA}|j\rangle - \langle i|\hat{\Sigma}(\epsilon)|j\rangle\right]^{-1}. \tag{5}$$

The dynamical correlation correction to the one-particle hamiltonian $H_{\rm LSDA}$ is represented via the energy-dependent self-energy operator $\hat{\Sigma}(\vec{r},\vec{r}\,',\epsilon)$ which in general is a non-local quantity. Here, the self-energy is calculated via the DMFT approach [16] that accounts only for local (on-site) correlations which are described within the Anderson impurity model (AIM) [21]. By linking the Green's function of the effective impurity to the single-site Green's function derived from the **k**-space summation DMFT provides the self-consistent method to determine the self-energy accounting for on-site correlations. The actual approximation made in DMFT is the substitution of the non-local (**k**-dependent) self-energy by the single on-site component. The latter corresponds to the limit of the infinite coordination. Fortunately, in many cases for 3-dimensional systems this is rather good approximation [22].

Although the formalism to be presented below is primarily used in connection with a site-diagonal self-energy, it should be stressed that any more complex self-energy can be used as well. In particular the formalism is able to deal with a site-non-diagonal self-energy occuring for example within the GW approach [23].

Dealing with crystals one can make use of Bloch's theorem when choosing basic functions $|i_{\mathbf{k}}\rangle$. This leads to the **k**-dependent Green's function matrix:

$$G^{\mathbf{k}}_{ij}(\epsilon) = \Big[\langle i_{\mathbf{k}}|j_{\mathbf{k}}\rangle\epsilon - \langle i_{\mathbf{k}}|\hat{H}_{\rm LSDA}|j_{\mathbf{k}}\rangle - \langle i_{\mathbf{k}}|\hat{\Sigma}(\epsilon)|j_{\mathbf{k}}\rangle\Big]^{-1}. \tag{6}$$

The efficiency and accuracy of the approach is determined by the choice of $|i_{\mathbf{k}}\rangle$. One of the most computationally efficient variational methods is the LMTO [24] which allows one to get a rather accurate description of the valence and conduction bands in the range of about 10 eV, which is enough for the calculation of the optical spectra ($\hbar\omega <$ 6-8 eV) . As the method introduces site- and angular momentum -dependent basis functions

$$\begin{aligned}\chi^{\mathbf{k}}_{lm\mathbf{R}}(\vec{r}) &= \Phi^{\rm h}_{lm}(\vec{r}-\mathbf{R}) \\ &+ \sum_{lm',\mathbf{R}'} h^{\mathbf{k}}_{lm\mathbf{R},lm'\mathbf{R}'}\Phi^{\rm t}_{lm'}(\vec{r}-\mathbf{R}')\,,\end{aligned} \tag{7}$$

it perfectly fits to any single-site approximation of the self-energy. The superscripts "h" and "t" stand for the so-called "head" and "tail" parts of the basis functions.

As the $\langle i|j\rangle$ and $\langle i|\hat{H}|j\rangle$ matrix elements in Eq. (6) are energy-independent it is enough to calculate them only once for each **k**-point.

In the framework of the DMFT the self-energy operator can be expressed in the form:

$$\hat{\Sigma}(\vec{r},\vec{r}\,',\epsilon) \;=\; \sum_{l,\mathbf{R}\mathbf{R}'} \delta_{\mathbf{R}\mathbf{R}'} \sum_{mm'} \Theta(|\vec{r}-\mathbf{R}|)\, Y^{*}_{lm}(\vec{r}-\mathbf{R}) \\ \times\; \Sigma^{\mathbf{R}\mathbf{R}'}_{lmm'}(\vec{r},\vec{r}\,',\epsilon)\; \Theta(|\vec{r}\,'-\mathbf{R}'|)\, Y_{lm'}(\vec{r}\,'-\mathbf{R}')\,, \tag{8}$$

where $\Theta(r) = 1$ if $\vec{r}$ is inside the atomic sphere and zero otherwise. Due to the special choice of LMTO basis functions (7) only the "head" component will give the significant contribution to the matrix elements of the self-energy operator (8) leading to an extremely simple **k**-independent expression:

$$\langle \chi^{\mathbf{k}}_{lm\mathbf{R}} | \hat{\Sigma} | \chi^{\mathbf{k}}_{lm'\mathbf{R}} \rangle \;\approx\; \int d^3r d^3r' \\ \times\; \Phi^{\mathrm{h}*}_{lm}(\vec{r}-\mathbf{R})\, \Sigma^{\mathbf{R}\mathbf{R}}_{lmm'}(\vec{r},\vec{r}\,',\epsilon)\; \Phi^{\mathrm{h}}_{lm'}(\vec{r}-\mathbf{R})\,. \tag{9}$$

The accuracy test of this approach was done in [13] and the error was found to be within 5% which is substantially less than the approximations made for the estimation of the self-energy itself.

The self-energy is calculated by using as an AIM-solver the so-called Spin-Polarised T-matrix plus Fluctuation Exchange (SPTF) approximation [25, 26]. SPTF is a perturbative appoach which provides an analytical technique to sum the infinite set of the Feynmann diagramms for the several types of interactions in the uniform electron gas. Fortunately these sets of diagrams very often appear to be sufficient to describe the effects caused by dynamical correlations in moderately-correlated shells like $3d$-electrons in transition metals [14, 27] as well as in systems with strong correlations [28]. This makes it a very attractive alternative to the so-called Quantum Monte-Carlo (QMC) technique [29] that sums all possible sets of diagramms of perturbation theory and therefore is much more time consuming.

The DMFT scheme is implemented within the KKR-GF method which allows to use the advantages of the scattering theory formulation in the Green's function construction. For example, it is possible to calculate the self-energy in a self-consistent manner (parallel with the charge density) [27].

Introducing the antihermitian part of the Green's function matrix (6) $\Im G_{ij} = \frac{1}{2}(G_{ij} - G^{\star}_{ji})$ and taking into account translational symmetry, the hermitian part of the optical

conductivity (2) is expressed as:

$$\sigma^{(1)}_{\lambda\lambda'} = \frac{1}{\pi\omega}\int d^3k \int_{\epsilon_F-\hbar\omega}^{\epsilon_F} d\epsilon \times \sum_{ij} \mathcal{J}^{\lambda}_{ij}(\mathbf{k},\epsilon)\mathcal{J}^{\lambda'}_{ji}(\mathbf{k},\epsilon+\hbar\omega) \tag{10}$$

with

$$\mathcal{J}^{\lambda}_{ij}(\mathbf{k},\epsilon) = \sum_n \Im G_{in}(\mathbf{k},\epsilon)\langle n_{\mathbf{k}}|\hat{J}^{\lambda}|j_{\mathbf{k}}\rangle\,. \tag{11}$$

Actually the possibility to split the $\mathcal{J}^{\lambda}_{ij}(\mathbf{k},\epsilon)$ matrix elements into the energy-dependent and -independent parts makes the calculation of optical conductivity rather fast.

The calculational procedure is built up as follows. The energy-dependent on-site self-energy $\Sigma(\epsilon)$ is obtained from the self-consistent KKR-GF scheme [27]. For a given self-energy the Dyson equation (6) is used to obtain the effective Green's function in the basis set of the LMTO method. The antihermitian part $\Im G_{ij}$ of the effective Green's function is used to calculate the matrix elements of the current-density operator in Eq. (11). The latter allows one to evaluate the optical conductivity given by Eq. (10). Spin-orbit coupling (SOC) which is together with exchange splitting the actual source of MOKE is taken into account via the second-variation technique.

The comparsion between the MO spectra of NiMnSb calculated within LSDA, LSDA+DMFT and the experimental results is shown in Fig. (1). The obvious conclusion is that an account of local correlations is essentially important to describe correctly the positions as well as the magnitudes of both low- and high-energy Kerr rotation peaks (situated at 1.4 eV and 4 eV).

It is sufficient to consider in details only the real part of the MOKE spectrum, i.e. the rotation, as the Kerr ellipticity is a related quantity.

The Mn *d*-shell indeed experiences noticable dynamical correlations as depicted by the self-energy plot shown in Fig. (2) with the amplitudes of the imaginary component up to 4 eV. For the Ni shell it is not so important the account of correlations as it is almost fully occupied. The effective Coulomb interaction is parametrised by $U = 3$ eV and $J = 0.9$ eV. Numerical tests show that approximately the same results are obtained within the range of $U = 3\pm0.5$ eV.

Considering Eqs. (10) and (11) we can straightforwardly analyse the modifications in the MO spectrum. As the matrix elements $\langle n_{\mathbf{k}}|\hat{J}^{\lambda}|j_{\mathbf{k}}\rangle$ are not influenced by DMFT, the two

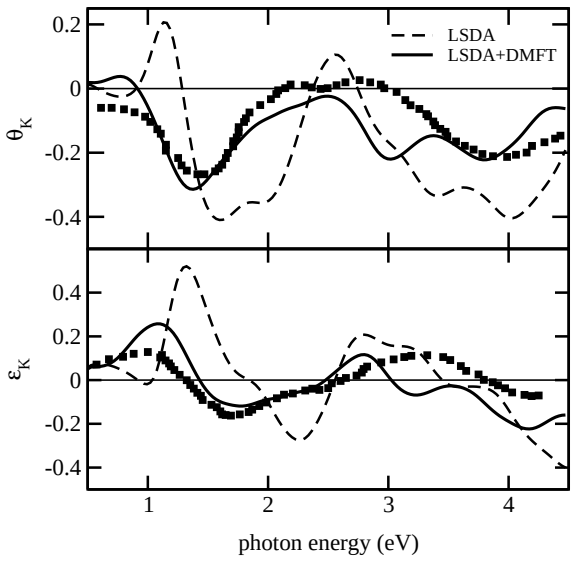

FIG. 1: MO spectra for NiMnSb. Upper panel: Kerr rotation angle; lower panel: Kerr ellipticity. Solid line: LSDA calculations; broken line: LSDA+DMFT calculations. The square points represent the experimental results given in Refs. [1, 2].

possible sources of the influence are the Green's function matrix and the change in the occupation numbers. However, in the present calculations the number of occupied and unoccupied states for each spin-projection is strictly conserved. This occurs due to the special construction of the self-energy represented by the so-called "particle-particle" channel [26]. The latter includes the channels of perturbation theory starting from the second-order and that is why pocessing the dominant contribution in the dynamical correlations for the d-electron shell. This leads in particular to the conclusion that local correlations modify only the interband part of the optical conductivity. The intraband contribution which is determined by the the Green's function matrix elements at the Fermi level remains unchanged. Thus, one can dominantly relate the changes in the Kerr effect to the modifications in the interband contribution of optical conductivity caused by the renormalisation of the one-particle spectrum which is shown in Fig. (3). The false peak inserted by DMFT at 3 eV could be attributed first of all to the lack of the vertex corrections in our calculational scheme. In order to describe the optical transitions correctly, the two-particle Green's function has to be used. That is because the expression (2) formulated in terms of the one-particle Green's function is an approximation which needs to be fullfilled with the appropriate vertex corrections [30]. However, the account of local correlations makes the implementation of vertex corrections in

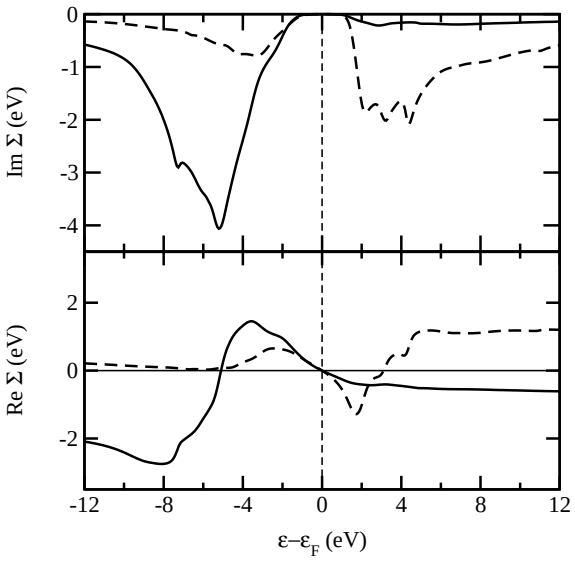

FIG. 2: Spin-resolved dynamical self-energy for Mn obtained from SPR-KKR calculations using SPTF solver. Lower panel: real component; upper panel: imaginary component. Solid and broken lines correspond to majority and minority spin-components respectively.

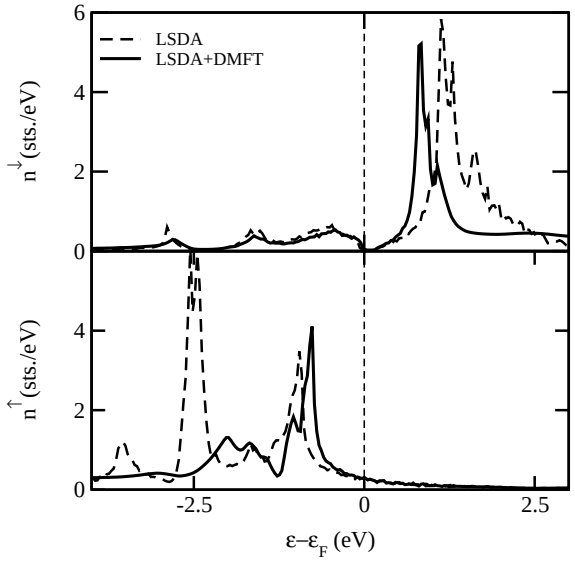

FIG. 3: Spin-resolved DOS of the Mn *d*-shell. Solid line: LSDA calculations; broken line: LSDA+DMFT calculations.

the computational scheme rather complicated and needs a separate investigation. Another aspect which might be interesting to investigate is the account of nonlocal correlations. In conclusion, it has been demonstrated that an improved description of correlation effects on the basis of the LSDA+DMFT scheme leads to a substantially improved agreement of the

theoretical and experimental MO spectra.

This work was funded by the German BMBF (Bundesministerium für Bildung und Forschung) under Contract No. FKZ 05 KS1WMB/1.

---

† Faculty of Science, University of Oradea, RO-410087 Oradea, Romania

[1] P. G. van Engen, K. H. J. Buschow, R. Jongebreur, M. Erman, Appl. Phys. Lett. **42**, 202 (1983).

[2] P. G. van Engen, Ph.D. thesis, Tech. Uni. Delft, 1983.

[3] R. Ohyama, T. Koyanagi and K. Matsubara J. Appl. Phys. **61**, 2347 (1987).

[4] P. P. J. van Engelen, D. B. de Mooij, J.H. Wijngaard and K. H. J. Buschow, J. Magn. Magn. Mat. **130**, 247 (1994).

[5] J. van Ek and J. M. Maclaren, Phys. Rev. B **56**, R2924 (1997).

[6] M. C. Kautzky, B. M. Clemens, Appl. Phys. Lett. **66**, 1279 (1995).

[7] P. M. Oppeneer, V. N. Antonov, T. Kraft, H. Eschrig, A. N. Yaresko, A. Y. Perlov, Solid State Comm. **94**, 255 (1995).

[8] V. N. Antonov, P. M. Oppeneer, A. N. Yaresko, A. Ya. Perlov, and T. Kraft, Phys. Rev. B **56**, 13012 (1997).

[9] X. Gao, J. A. Woollam, R. D. Kirby, D. J. Sellmyer, C. T. Tanaka, J. Nowak, J. S. Moodera, Phys. Rev. B **59**, 9965 (1999).

[10] S. Picozzi, A. Continenza, A. J. Freeman, J. Phys. D: Appl. Phys. **39**, 851 (2006).

[11] E. T. Kulatov, Y. A. Uspenskii, S. V. Halilov, Phys. Lett. A **125**, 267 (1994).

[12] Y. A. Uspenskii, E. T. Kulatov, S. V. Khalilov, JETP **80**, 952 (1995).

[13] A. Perlov, S. Chadov, H. Ebert, Phys. Rev. B **68**, 245112 (2003).

[14] A. Perlov, S. Chadov, H. Ebert, L. Chioncel, A. I. Lichtenstein, M. I. Katsnelson, J. Magn. Magn. Matter. **272**, 523 (2004).

[15] L. Chioncel, M. I. Katsnelson, R. A. de Groot, and A. I. Lichtenstein, Phys. Rev. B **68**, 144425 (2003).

[16] A. Georges, G. Kotliar, W. Krauth and M. J. Rozenberg, Rev. Mod. Phys. **68**, 13 (1996); G. Kotliar and D. Vollhardt, Phys. Today **57** (3), 53 (2004).

[17] J. L. Erskine, E. A. Stern, Phys. Rev. B **12**, 5016 (1975).

[18] L. Szunyogh and P. Weinberger, J. Phys.: Condensed Matter **11**, 10451 (1999).

[19] R. Kubo, J. Phys. Soc. Japan **12**, 570 (1957); D.A. Greenwood, Proc. Phys. Soc. **71**, 585 (1958).

[20] T. Huhne, C. Zecha, H. Ebert, P. H. Dederichs, R. Zeller, Phys. Rev. B **58**, 10236 (1998).

[21] P. W. Anderson, Phys. Rev. **124**, 41 (1961).

[22] W. Metzner, D. Vollhardt, Phys. Rev. Lett. **62**, 324 (1989).

[23] S. Biermann, F. Aryasetiawan, A. Georges, Phys. Rev. Lett. **90**, 086402-1 (2003).

[24] O.K. Andersen, Phys. Rev. B **12**, 3060 (1975).

[25] N. E. Bickers and D. J. Scalapino, Ann. Phys. (NY) **193**, 206 (1989).

[26] A. I. Lichtenstein and M. I. Katsnelson, Phys. Rev. B **57**, 6884 (1998); M. I. Katsnelson and A. I. Lichtenstein, J. Phys.: Condens. Matter **11,** 1037 (1999); M. I. Katsnelson and A. I. Lichtenstein, Eur. Phys. J. B **30**, 9 (2002).

[27] J. Minar, L. Chioncel, A. Perlov, H. Ebert, M.I. Katsnelson, A.I. Lichtenstein Phys. Rev. B **72**, 045125 (2005).

[28] L. V. Pourovskii, M. I. Katsnelson, A. I. Lichtenstein, Phys. Rev. B **72**, 115106 (2005).

[29] J. E. Hirsch, R. M. Fye, Phys. Rev. Lett. **56**, 2521 (1986); K. Held, I. A. Nekrasov, N. Blümer, A. Anisimov, D. Vollhardt, Int. J. Mod. Phys. B **15**, 2611 (2001).

[30] G. Mahan, *Many-Particle Physics* (Plenum Press, New York, 1990), Chap. 8.